ARTICLES

Fractionation of Multiwalled Carbon Nanotubes by Cascade Membrane Microfiltration

Thomas Abatemarco,[†] Jonathan Stickel,[†] Jonathan Belfort,[‡] Brian P. Frank,[†] P. M. Ajayan,*[,‡] and Georges Belfort*[,†]

Howard P. Isermann Department of Chemical Engineering, Department of Materials Science and Engineering, Rensselaer Polytechnic Institute, Troy, New York 12180

Received: October 8, 1998; In Final Form: February 26, 1999

Multiwalled carbon nanotubes were purified and size-separated by a multistep microfiltration process through a sequence of track-etched polycarbonate membranes of various pore sizes in both dead-ended and cross-flow mode. For this cascade microfiltration, the electric arc derived raw multiwalled samples were suspended in an aqueous solution of sodium dodecyl sulfate in deionized water. By examining the deposits on the membrane surfaces and in the permeate suspensions with scanning electron microscopy and atomic force microscopy, the nanotube fractionation was confirmed and analyzed. These scanning techniques showed that the components of the crude sample, which included carbon nanotubes, polyhedral nanoparticles, and large aggregates, were separated from each other during the filtration. In addition, fractionation of the multiwalled carbon nanotubes according to length was possible.

Introduction

Multiwalled carbon nanotubes are assemblies of concentric sp^2 bonded carbon tubules made of rolled-up graphite sheets. All the tubules are capped at the ends by hemispherical fullerene-like structures.[1] Carbon nanotubes are becoming technologically important materials with proposed uses ranging from electronic devices[2,3] to catalytic supports for reactions such as those important in fuel cells,[4,5] advanced AFM tips,[6] filler material for superconducting materials[7] and polymers,[8] storage of gases,[9] metals,[10] topographical imaging and molecular manipulation,[11] and even with DNA.[12]

The multiwalled nanotubes (MWNT) that we observed tended to be typically between 5 and 30 nm in diameter and up to several microns in length. The MWNT studied here were generated by the well-established electric arc discharge technique.[1] In addition to carbon nanotubes, the sample contained carbon nanoparticles (multilayered particles with sizes typically between 10 and 30 nm) and large aggregates of these spheres. To separate nanotubes from impurities (nanoparticles and aggregates) and obtain the high aspect ratio that is important for many applications, previous researchers have used chemical methods such as oxidation to etch away impurities,[13] size exclusion chromatography to fractionate MWNT,[14] and microfiltration techniques to purify single-walled carbon nanotubes.[15] In the research described here, we have optimized a multistep microfiltration method with membranes of narrow pore size distribution to separate the nanotubes from impurities and also to fractionate the nanotubes by length.

* Authors to whom correspondence should be addressed.
[†] Howard P. Isermann Department of Chemical Engineering.
[‡] Department of Materials Science and Engineering.

Methods and Materials

An aqueous solution of 1 wt % sodium dodecyl sulfate (SDS) surfactant and sonication were used to break up and suspend the nanotube bulk sample for fractionation. SDS has previously been used to reduce aggregation and suspend nanotubes for fractionation.[14] Polycarbonate track-etched membranes (Nucleopore, Pleasanton, CA) were used because of their cylindrical pore geometry and extremely narrow pore size distribution. The filtration process was conducted using 8, 5, 3, 1, 0.8, 0.6, 0.4, 0.2, and 0.1 μm rated pore diameter membranes in sequence from largest to smallest pore diameter. Two different filtration systems were used to fractionate the MWNT: a dead-end system and a cross-flow system.

The dead-end system, with flow perpendicular to the membrane, is shown in Figure 1a,b. It used a 50 mL stirred ultrafiltration cell (#8050, Amicon Division, Millipore Corporation, Bedford, MA) loaded with a circular piece of membrane having a diameter of about 43 mm and a filtration surface area of 14.2 cm^2. The cell had discrete high and low permeate flux regions due to the presence of solid supports underneath half of the membrane surface and empty channels under the other half. Between 2 and 3 mg of crude MWNT was suspended in 5 mL of 1 wt % SDS (aq) and sonicated for about 20 min. The membrane was washed and permeated with 5 mL of the SDS solution, then the MWNT suspension was filtered through the membrane under about 50 kPa compressed N_2 pressure. The membrane was then washed and permeated with 5 mL of ethanol to remove any excess SDS, and dried in a vacuum oven (−100 kPa, about 30° C). This process was repeated for each membrane in the sequence, where the permeate from each step was sonicated for 2 min to ensure that all the carbon material was well suspended. A drop of the final permeate of the 0.1 μm

10.1021/jp984020n CCC: $18.00
Published on Web 04/15/1999

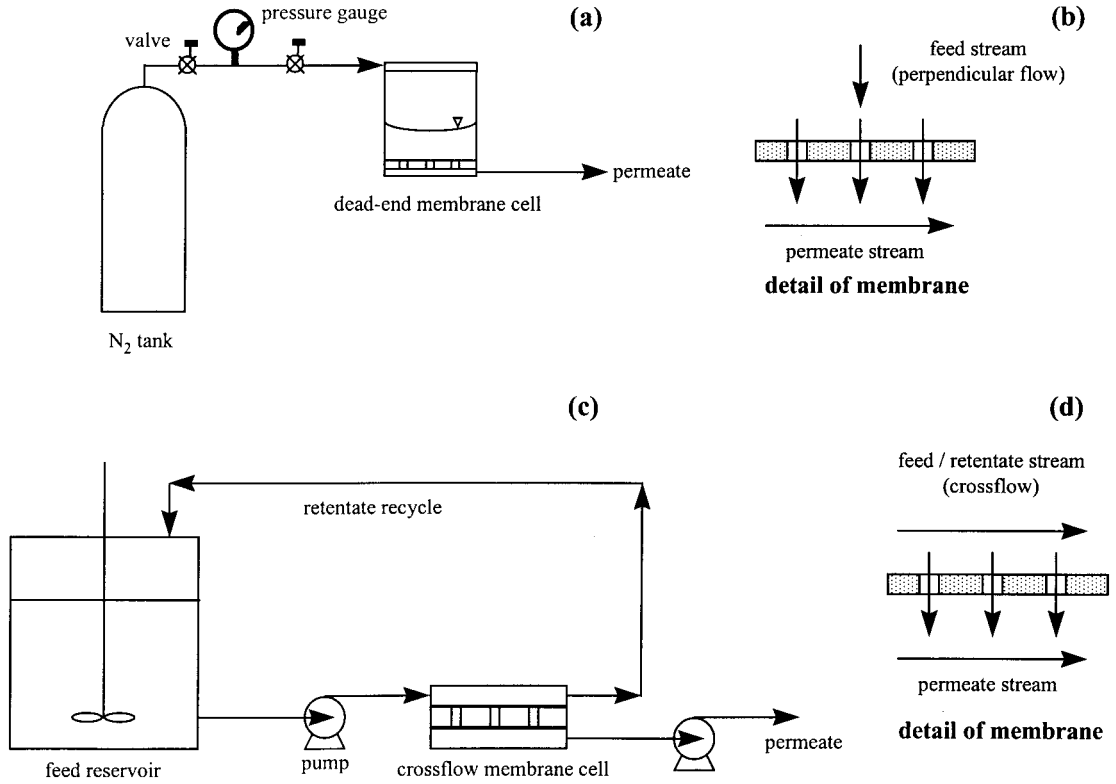

Figure 1. Flow diagrams of (a) the dead-end filtration system with (b) flow perpendicular to the surface and (c) cross-flow filtration system with (d) flow parallel to the surface.

membrane was placed on a silicon wafer, dried in the vacuum oven, and washed with ethanol to remove excess SDS.

The cross-flow system, with bulk flow parallel to the membrane, is shown in Figure 1c,d. It used a cell (Minitan system, Millipore) suitable for an 11 cm long by 6 cm wide membrane. The cell had two plates: the lower one connected to the feed and retentate streams, and the upper one connected to the permeate stream. The plates were separated by a silicone retentate separator (#PSSP0MT11, Millipore), and all streams were connected via Tygon tubing (Pharmed 6485-16, Masterflex, Cole-Parmer, Chicago, IL). The feed stream was pumped into the cell by a peristaltic pump with pump head 7518-10 (Masterflex), and the permeate stream was pumped from the cell by a similar pump with a different pump head (7018-20, Masterflex). The final assembly had a membrane filtration surface area of 43.2 cm^2 and 36 cross-flow channels, each having a cross-sectional area of 1 mm^2. The cross-flow channels were all connected to an inlet and outlet manifold. About 30 mg of crude MWNT was suspended in 50 mL of 1 wt % SDS (aq) and sonicated for about 30 min. The membrane was washed and permeated by 10 mL of the SDS solution at a volumetric flow rate of about 0.375 mL/s, then the MWNT suspension was filtered through the membrane with a feed stream of 1.125 mL/s, a permeate stream of 0.6 mL/s, and a retentate (recycle) stream of 0.525 mL/s. The membrane was then washed and 10 mL of ethanol at 0.375 mL/s was passed through to remove any excess SDS, and dried in the same vacuum oven. As with the dead-end system, this process was repeated for each membrane in the sequence, with the permeate of each step being sonicated for 5 min to ensure that all the carbon material was well suspended. Again, a drop of the final permeate from the 0.1 μm membrane was placed onto a silicon wafer, dried in the vacuum oven, and washed with ethanol.

To analyze the samples, the silicon wafers and sections of the used membranes were imaged using both SEM (Field Emission JSM-6300F, JEOL, Japan) and AFM (Autoprobe CP, Park Scientific Instruments, Sunnyvale, CA). SEM and AFM were used as complimentary techniques. SEM yields a faster, larger view of the substrate, whereas AFM yields atomic resolution images and better measurement for dimensional analyses. Also, SEM of these samples required a metal layer to be deposited on the sample surface. This metal layer had about the same thickness as one dimension of the particles to be imaged. For these reasons SEM was used to view the overall filtration characteristics of the membranes while AFM was used to determine actual dimensional data. All AFM images were taken in contact mode at a rate of 1 Hz using Type A sharpened microlevers (Park Scientific) with a tip radius of 20 nm. Sizes were measured using the AFM's image analysis software. Also, several runs were conducted using both filtration systems for comparison.

The amount of MWNT, polyhedral aggregates, and large aggregates in the initial sample varied widely, making determining the efficiency of the filtration process problematic. In addition, the amount of material recovered by each membrane was too small to be measured by direct weighing. Qualitative evaluations of the density of particles on each membrane were made on the basis of the SEM and AFM images.

Results

Three runs were conducted with the full cascade of membranes (8, 5, 3, 1, 0.8, 0.6, 0.4, 0.2, and 0.1 μm rated pore sizes) and the dead-end cell. AFM images of the surfaces of the 8 and 5 μm pore size membranes after filtration indicated that these membranes stopped all of the large aggregates. While a few tubes and spheres did appear on these membranes, their density was very low. Since the aggregates made these surfaces very rough, the AFM tip tended to slip and shift objects on the surface while scanning, so imaging was difficult. The deposits

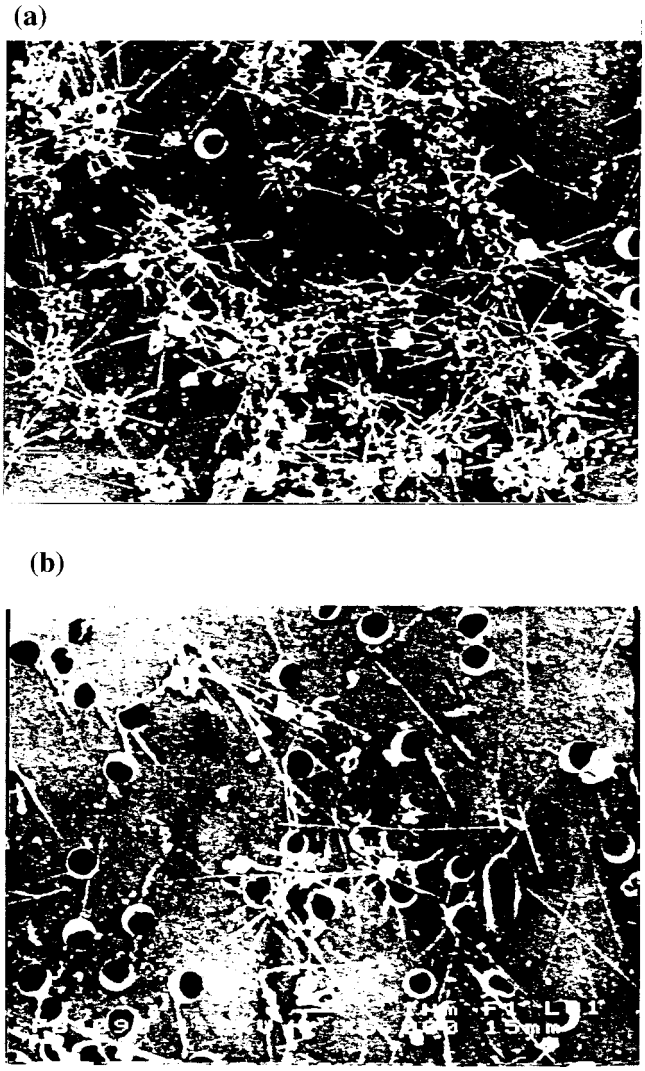

Figure 2. Two different SEM images (a and b) of the surface of the 1.0 μm pore size membrane after dead-end filtration of the nanotube suspension, showing a large number of nanotubes and their localization near the pores.

on the 3 μm pore size membranes were the first in the sequence to indicate the presence of isolated carbon nanotubes in high densities. Both average-sized (about 2−3 μm in length) and very long nanotubes up to 12 μm in length were present on these surfaces (size measurements will be discussed later), along with a fairly low density of nanoparticles. These scans also indicated that both tubes and spheres tended to be localized near the pores, a trend that was observed for all of the membrane sizes.

Localization of tubes near the pores was also apparent in images of the deposit on the 1 μm pore size membranes. These membranes consistently displayed the highest density of tubes and a very low density of spheres, and the SEM images in Figure 2a,b clearly show both this distribution and the localization of material near the pores. These observations are confirmed by the AFM scans in Figure 3a,b, which also indicate a high degree of flexibility of the tubes, twisting around each other to form "knots" and curving into the pores.

The material on the 0.8, 0.6, and 0.4 μm pore size membranes all had similar properties. There was an intermediate density of tubes localized near the pores with very few if any spheres present. Like the 0.8 μm pore size membrane, the deposits on both the 0.6 and the 0.4 μm pore size membranes were nanotubes localized at the pores and a very low density of spheres, many of which are associated with the tubes. While

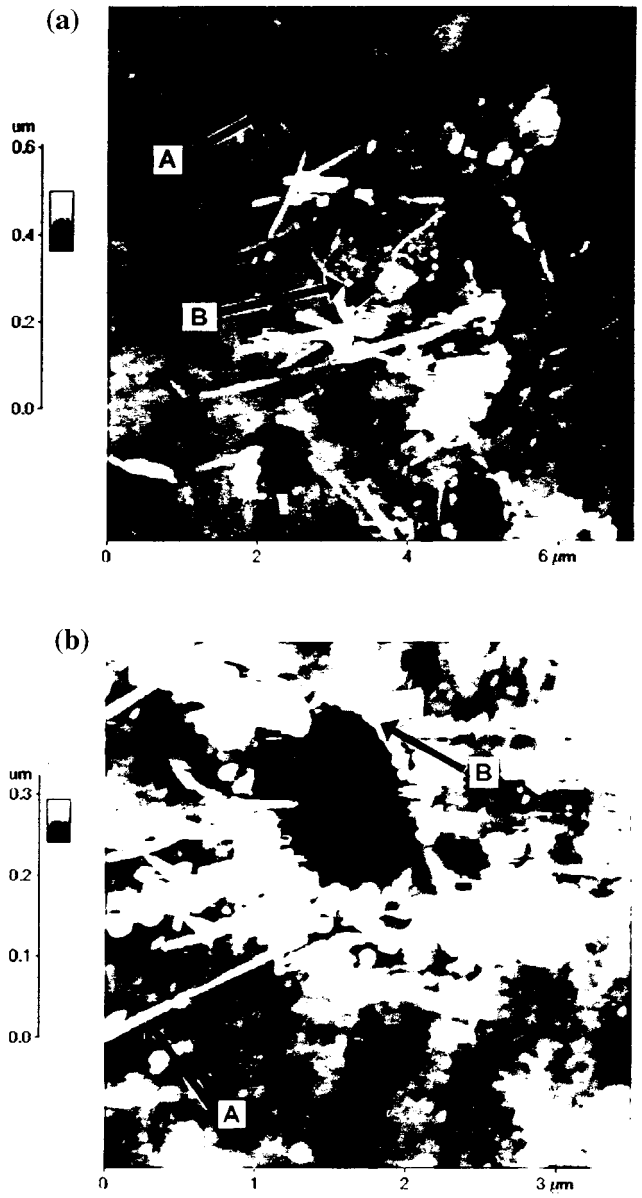

Figure 3. Two different AFM images (a and b) of the surface of the 1.0 μm pore size membrane shown in Figure 2. From these close-up images of regions near pores, nanotubes (A) and nanoparticles (B) are clearly evident. Contrast on the image indicates height of features as shown on scale at the left.

the deposits on the 0.8, 0.6, and 0.4 μm pore size membranes have very similar density distributions of the different species, the tubes present noticeably decreased in size (both diameter and length) with decreasing membrane pore size. To a lesser extent, spheres also show a similar size gradient. In addition, the tube and sphere diameters appear to be correlated. The graph in Figure 4, which summarizes the size measurements taken for the full sequence of membranes in the dead-end cell for all three runs, indicates these trends.

For the 0.2 μm pore size membrane, practically all of the carbon material present was in the form of nanoparticles (spheres). While a few tubes were present, the high density of nanoparticles overwhelmed them. The deposit on the 0.1 μm pore size membrane also showed a very high density of spheres (the 0.2 and 0.1 μm pore size membranes retained a vast majority of the nanoparticles), and no other species were detected at this pore size. The final permeate samples also displayed only nanoparticles, but these spheres were the smallest and were at a very low density.

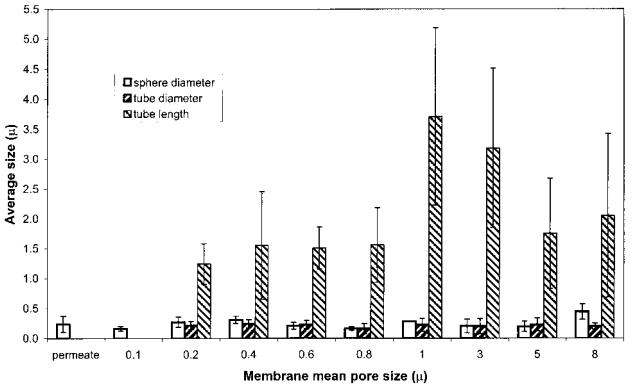

Figure 4. Size distribution of nanoparticles (open columns), nanotube diameters (right diagonal hatching), and nanotube lengths (left diagonal hatching) for 0.1 to 8 μm pore size membranes and the permeate from dead-end microfiltration. All dimensions were determined from the AFM images.

To decrease the time and complexity of the experiment, and with scale-up considerations in mind, a run was conducted using only the 3, 0.6, and 0.2 μm membranes in both the dead-end and cross-flow filtration systems. In this experiment, neither filtration cell successfully separated the species in the crude MWNT sample, probably because the smaller number of membranes in the sequence meant that more material was deposited on each membrane, causing intense fouling. This result indicated that the full sequence of membranes was necessary to achieve fractionation of the nanotubes on a significant scale.

Several major differences were observed between the results of the full cascade in the dead-end cell and the cross-flow system. One observation is the absence of large aggregates in the deposits on the membranes used in the cross-flow system. Aggregation of the various particles in the sample can occur during convective drag toward the membrane as the particles approach one another and overcome electrostatic repulsion, forming an aggregate. A possible reason for the absence of aggregates in the cross-flow system is the existence of particle lift effects which include inertial lift and shear-induced diffusion. For these cases, the lift away from the membrane is proportional to the particle diameter to the third and four thirds power, respectively. Without cross-flow these particle lift effects are absent.[16]

Nanotubes were also obtained in much higher purity in the cross-flow cell. No nanoparticle impurities were present in the deposits on membranes with pore sizes from 0.4 to 1 μm, while nanotubes were present throughout that range, and in very high density on the 1 and 0.6 μm pore size membranes, as the AFM scans of the deposits on the 1 μm membrane in Figure 5 show. Also, the size distribution graph in Figure 6 indicates that tube sizes (both length and diameter) decreased even more regularly with decreasing membrane pore size than they had in the dead-end cell, displaying an even better fractionation of the tubes by size.

Discussion

In general, all large aggregates in the samples were retained by the 8 and 5 μm pore size membranes and all MWNT were retained on the 3 to 0.2 μm pore size membranes. Almost all of the nanoparticles appeared on the 0.2 μm and smaller pore size membranes and in the final permeate. However, some species did appear on membranes earlier in the sequence than expected. For example, a few tubes appeared on the 8 μm pore size membrane even though their lengths were far below 8 μm,

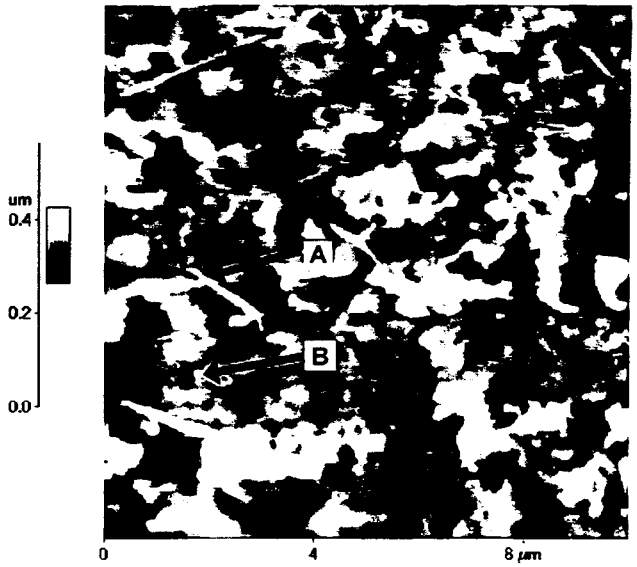

Figure 5. AFM image of the surface of the 1.0 μm pore size membrane after cross-flow filtration of the nanotube suspension. Note the high and low density of nanotubes (A) and nanoparticles (B), respectively. Contrast on the image indicates height of features as shown on the scale at the left.

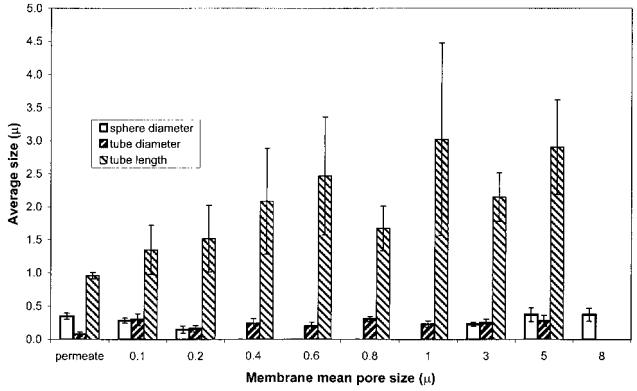

Figure 6. Size distribution of nanoparticles (open columns), nanotube diameters (right diagonal hatching) and nanotube lengths (left diagonal hatching) for 0.1 to 8 μm pore size membranes and the permeate from cross-flow microfiltration. All dimensions were determined from AFM images.

and some spheres appeared throughout the entire sequence although no spheres or aggregates were larger than 0.4 μm in diameter. These differences must have been due to fouling of the membrane (a high density of material closed-off the pores decreasing permeation flux through the membrane and retaining particles that would otherwise have passed through) and the ability of particles in the dead-end cell to be dragged to the surface by permeate flux and adhere to the surface because of interception and adhesion. The purpose of the cross-flow system was to alleviate these problems through both a higher shear stress at the membrane surface and reentrainment of particles back to the retentate.[16]

As Figure 6 shows, tubes tended to decrease in size with decreasing pore sizes. Some conclusions can be made from these data regarding the orientations of the tubes as they pass though the membranes in the sequence. Most tubes could easily pass through the 8 and 5 μm pore size membranes because they were less than 5 μm in length. Most tubes greater than 3 μm were retained by the 3 μm pore size membrane. The 1 μm pore size membrane had the greatest density of tubes because practically all of the tubes in the sample were greater than 1 μm in length,

so any tube that approached the surface nearly parallel to the membrane was trapped. However, many tubes were still able to pass through the 1 μm pore size membrane because the permeate flux aligned them along the stream lines with their long axis parallel to the pore axis (although their length was greater than 1 μm, their diameter was generally between 5 and 30 nm, allowing them to pass through easily). The same behavior occurred on the 0.8, 0.6, and 0.4 μm membranes, with smaller tubes having a greater chance of passing through, thus causing the observed size gradient.

Because fractionation of either species or sizes was not accomplished with a partial range of membranes, the full range of membranes was necessary for effective fractionation. The partial sequence was probably ineffective because of fouling (pore plugging and surface deposition) caused by the high density of the suspended material. Each of the smaller number of membranes was exposed to a large amount of material that blocked the pores, which prevented any useful separations from occurring.

Filtration using the cross-flow system was much more effective than the dead-end system. The cross-flow cell allowed for about 10 times as much material to be fractionated and nanotubes of much higher purity were captured. As Figure 6 shows, the cross-flow system also obtained a more regular tube size gradient than that observed in the dead-end cell (Figure 4), which means that the crude sample was fractionated both by species and by size more effectively in the cross-flow filtration. It may be possible to further improve the filtration performance of the cross-flow system by optimizing the hydrodynamic parameters.

Acknowledgment. We acknowledge the support of the US. Department of Energy, Basic Chemical Sciences Division (Grant No. DE-FG02-90ER14114) and the National Science Foundation (Grant No. CTS-9400610). We also thank Benjamin H. Carter of Corning Incorporated Separations Division, Acton, MA for supplying some of the track-etched membranes. P. M. Ajayan acknowledges the ACS Petroleum Research Grant for funding and Frau Sabine Kuhnemann for operation of the SEM at the Max-Planck-Institute für Metallforschung, Stuttgart, Germany.

References and Notes

(1) Ebesen, T. W.; Ajayan, P. M. *Nature* **1992**, *358*, 220.
(2) Dresselhaus, M. S. *Nature* **1998**, *391*, 19.
(3) White, C. T.; Todorov, T. N. *Nature* **1998**, *393*, 240.
(4) Planeix, J. M.; Coustel, N.; Coq, B.; Brotons, V.; Kumbhar, P. S.; Dutartre, R.; Geneste, P.; Bernier, P.; Ajayan, P. M. *J. Am. Chem. Soc.* **1994**, *116*, 7935.
(5) Che, G.; Lakshmi, B. B.; Fisher, E. R.; Martin, C. R. *Nature* **1998**, *393*, 346.
(6) Dai, H.; Hafner, J. H.; Rinzler, A. G.; Colbert, D. T.; Smalley, R. E. *Nature* **1996**, *384*, 147.
(7) Fossheim, K.; Ebbesen, T. W. U.S. Patent 5,627,140, May, 1995.
(8) Chellappa, V.; Chiou, Z. W.; Jang, B. Z. *J. Mater. Sci.* **1995**, *30*, 4263.
(9) Rodriguez, N. M.; Baker, T. K. U.S. Patent 5,653,951, May, 1995.
(10) Yamamoto, K.; Funasaka, H.; Takahashi, T.; Suzuki, T.; Marayama, Y.; Kato, T.; Akasaka, T. U.S. Patent 5,717,076, September, 1998.
(11) Wong, S. S.; Joselevich, E.; Woolley, A. T.; Cheung, C. L.; Lieber, C. M. *Nature* **1998**, *394*, 52.
(12) Tsang, S. C.; Guo, Z.; Chen, Y. K.; Green, M. L. H.; Hill, H. A. O.; Hambley, T. W.; Sadler, P. J. *Angew. Chem., Int. Ed. Engl.* **1997**, *36*, 2197.
(13) Hiura, H.; Ebbesen, T. U.S. Patent 5,698,175, July, 1995.
(14) Duesberg, G. S.; Burghard, M.; Muster, J.; Philip, G.; Roth, S. *Chem. Commun.* **1998**, 435.
(15) Bandow, S.; Rao, A. M.; Williams, K. A.; Thess, A.; Smalley, R. E.; Eklund, P. C. *J. Phys. Chem. B* **1997**, *101*, 8839.
(16) Belfort, G.; Davis, R.; Zydney, A. L. *J. Membr. Sci.* **1994**, *96*, 1.